J. Fluid Mech. (2012), *vol.* 706, *pp.* 274–294.
doi:10.1017/jfm.2012.253

On the flow of buoyant fluid injected into an aquifer with a background flow

Iain Gunn and Andrew W. Woods†

BP Institute for Multiphase Flow, University of Cambridge, Madingley Road, Cambridge CB3 0EZ, UK

(Received 23 December 2010; revised 10 April 2012; accepted 24 May 2012;
first published online 12 July 2012)

We study the dispersal of a plume of incompressible buoyant fluid injected into a confined inclined aquifer in which there is a background flow. We assume that, to prevent pressure buildup in the system, there is an outflow from the aquifer, with flux equal to the injection flux, through a producing well. Using the method of characteristics, we identify that the trajectory of the plume of injected fluid depends on the magnitudes of both the injection flux Q_I and the background aquifer flux Q_A relative to the buoyancy-driven exchange flow of injected and original fluid within the aquifer Q_E, on the direction of the background aquifer flow, and on whether the producing well lies upslope or downslope from the injecting well. We find the values of the controlling parameters Q_I/Q_E and Q_A/Q_E for which all injected fluid flows up-dip, for which the injected fluid partitions into a component moving up-dip and a component moving down-dip, and for which all injected fluid flows down-dip. A key learning from the analysis is that there may be very different plume trajectories when a buoyant fluid is injected into a confined, inclined aquifer, and prediction of the trajectory depends on knowledge of the background flow as well as the injection rate and location of the producing wells. In the process of CO_2 sequestration, this range of initial plume geometries can inform analysis of longer-term geological storage and assessment of the risk of activating different possible leakage pathways to the surface.

Key words: porous media, gravity currents, convection in porous media

1. Introduction

There is growing interest in the process of carbon capture and storage (CCS) for its potential role in reducing carbon dioxide (CO_2) emissions into the atmosphere. Numerous studies have been carried out to explore the physical processes that control the migration of CO_2 following injection into deep subsurface aquifers (e.g. Pruess *et al.* 2003; Juanes *et al.* 2006; Bickle *et al.* 2007; Hesse, Orr & Tchelepi 2008). One of the key objectives of such modelling is to quantify the mechanisms and time scales associated with the possible migration of CO_2 back to our environment (Nordbotten *et al.* 2009).

It has been shown that, if the aquifer is of large vertical extent compared with the depth of the CO_2 current, the motion of the original fluid in the aquifer is of secondary importance to the flow (Barenblatt 1996; Hesse *et al.* 2008). Many studies have focused on the long-time dispersal of the CO_2 when this limit of a gravity-driven thin flow is appropriate (e.g. Nordbotten & Celia 2006; Vella & Huppert 2006; Hesse *et al.* 2008; Farcas & Woods 2009; Neufeld, Vella & Huppert 2009). Such models

† Email address for correspondence: andy@bpi.cam.ac.uk

have explored the role of capillary trapping (Hesse *et al.* 2008), leakage through the cap rock (Farcas & Woods 2009) and dissolution (Neufeld *et al.* 2010) on the long-time evolution of the CO_2 plume.

In contrast to the dynamics of the dispersal of CO_2 at long times, during the initial injection phase the dynamics of the displaced ambient water can also be significant, particularly if the height of the aquifer is sufficiently small that it is effectively 'confined'. A two-layer flow results, with a dynamic pressure gradient in both the CO_2 and water (Mitchell & Woods 2006; Nordbotten & Celia 2006; Hesse *et al.* 2008; Gunn & Woods 2011).

A governing equation for such displacement of one fluid by a second in a confined, inclined aquifer in a two-dimensional geometry was originally developed by Bear (1988, § 9.5.5), assuming that the interface remains sharp. Hesse *et al.* (2008) found solutions for this system for the case in which a finite volume of CO_2 spreads through the aquifer following injection, drawing from the work of Yortsos (1995) to motivate the use of the sharp-interface simplification based on the vertical-equilibrium approximation for a flow with a narrow capillary transition zone. Woods & Norris (2010) also discuss the value of sharp-interface models, in the context of gas plumes. Mitchell & Woods (2006) and Nordbotten & Celia (2006) explored the dynamics of the two-layer flows that develop when one fluid is injected into a horizontal, laterally extensive confined aquifer from a vertical well, showing that the model solutions compare well with some small-scale laboratory experiments.

During the injection phase of the sequestration process, as the system is pressurized, faults may develop or be reactivated within the seal rock above the permeable aquifer. These may then provide a possible pathway for CO_2 to leak from the reservoir. In a recent study Gunn & Woods (2011) explored how such leakage can impact the dynamics of a confined flow of buoyant fluid in an inclined aquifer. Their modelling showed the flow patterns that can develop in an aquifer of finite lateral extent, bounded both up-dip (upslope) and down-dip (downslope) by faults. They explored the cases in which either the fault up-dip or the fault down-dip of the injection well is permeable, thereby providing an outflow pathway for the water displaced by the injection of CO_2. They demonstrated that there are a range of different patterns of flooding and associated storage efficiencies depending on whether the injection well is located up-dip or down-dip from the fault.

However, in many aquifer systems there is also a natural groundwater flow, which we call a 'background' flow, which imposes a large-scale pressure gradient on the system. Juanes, MacMinn & Szulczewski (2010) have recently explored the role of such a background flow on the migration of a finite plume of CO_2 moving through a confined aquifer, following injection. However, the sensitivity of the system to the far-field flux conditions demonstrated by Gunn & Woods (2011) motivates us to explore the role of such a background flow during the injection of a plume of CO_2, and this is the main topic of the present paper. We generalize the approach of Bear (1988) to account for the presence of a background flow and examine the motion of the injected plume; in our analysis, we include a production well (or leaking fault) either up-dip or down-dip from the point of injection, as may be included in the design of a CO_2 injection system to prevent reservoir pressure from becoming too large during injection.

We initially consider the case in which the producing well lies up-dip from the injecting well (see figure 1): in § 2 we develop the model, in § 3 we present analytical solutions describing the long-time asymptotic behaviour of the system, and in § 4 we compare these results with numerical solutions of the full governing equations. In

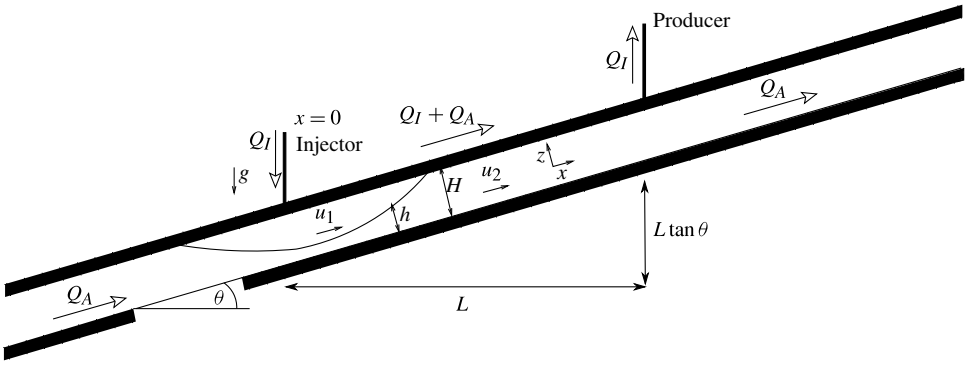

FIGURE 1. Diagram of the modelled layer.

§ 5 we then consider the case in which the producing well lies down-dip from the injecting well, illustrating the different dependence of the flow morphology on the controlling parameters in this case. In § 6 we consider implications of the work for practical CO_2 injection scenarios.

2. The model

Our analysis assumes incompressible flow, building on the original approach of Bear (1988) and Hesse *et al.* (2008). The analysis is framed in a two-dimensional geometry, as is appropriate for the case of injection from a long horizontal well aligned in the cross-slope direction, or for the large-scale flow associated with a series of vertical wells arranged along a line in the cross-slope direction. We consider times after the current has spread far from the injection well, when the assumption that the flow is parallel to the base of the layer may be applied (Nordbotten & Celia 2006; Pritchard 2007; Hesse *et al.* 2008). We consider the evolution of the plume until such time as the leading edge of the current of injectate reaches the producing well or fault through which outflow takes place. We also assume that there is a sharp interface between the fluids, and that the motion is governed by Darcy's law.

The modelled geometry is illustrated in figure 1, where x is the spatial coordinate in the up-dip direction, at small angle θ to the horizontal, and z is the position above the base of the layer, measured perpendicular to the slope (i.e. at angle θ to the vertical). We assume that the buoyant fluid is introduced at the top of the aquifer at the point $x = 0$, at a rate Q_I m^2 s^{-1} per unit distance cross-slope. The aquifer is assumed to have depth H, lateral extent $L \gg H$ between the wells, and inclination $\theta \ll 1$ to the horizontal. As a simplification to aid analysis of the far-field motion, the injecting well is treated as a point source of fluid located at $x = 0$.

We assume also that the evolving buoyant current occupies the region $h(x, t) < z < H$, and has viscosity μ_1 and density ρ_1. The ambient fluid, which occupies the region $0 < z < h(x, t)$, has viscosity $\mu_2 > \mu_1$ and density $\rho_2 = \rho_1 + \Delta\rho$.

We consider injection rates Q_I such that the dynamic pressure gradient satisfies

$$\frac{kQ_I}{2\pi\mu H^2} \ll \Delta\rho g \cos\theta, \tag{2.1}$$

so that the cross-layer component of the buoyancy dominates the radial pressure gradient associated with the injection, and so over a region of lateral extent H any

variation in the depth of the fluid–fluid interface Δh is small,

$$\frac{\Delta h}{H} \sim \frac{kQ_I}{2\pi\mu\Delta\rho g\cos\theta H} \ll 1. \tag{2.2}$$

In the following analysis, we are therefore able to partition the flux into an up-dip and a down-dip component while assuming that the depth of the flux at the source is continuous. In the limit

$$\frac{\mu Q_A}{kH} \ll \Delta\rho g, \tag{2.3}$$

where Q_A is the flux of the background flow, the cross-slope component of gravity dominates the along-slope pressure gradient associated with the background flow, and so, given (2.1), any transitions in the depth of the flow occur over along-aquifer length scales $x \gg H$, and so everywhere the flow remains approximately parallel to the boundary. That is, the pressure in the z direction is approximately hydrostatic, being given by

$$p(x, z, t) = p_0(x, t) - \rho_2 gz\cos\theta \tag{2.4}$$

for $0 < z < h$ and by

$$p(x, z, t) = p_0(x, t) - \Delta\rho gh\cos\theta - \rho_1 gz\cos\theta \tag{2.5}$$

for $z > h$, where $p_0(x, t)$ is the pressure on the lower boundary of the permeable layer. Darcy's law then leads to the relations

$$u_1 = -\frac{k_1}{\mu_1}\left(\frac{\partial p_0}{\partial x} - \Delta\rho g\cos\theta\frac{\partial h}{\partial x} + \rho_1 g\sin\theta\right), \tag{2.6}$$

$$u_2 = -\frac{k_2}{\mu_2}\left(\frac{\partial p_0}{\partial x} + \rho_2 g\sin\theta\right), \tag{2.7}$$

where u_1 and u_2 are the transport velocities of the injectate and the ambient fluid, respectively, in the up-dip sense (cf. Gunn & Woods 2011).

To complete the model for the flow, we specify conditions for mass conservation. We assume that the producing well lies up-dip from the injecting well and produces a flux equal to the injection flux Q_I, and that the aquifer has a background flux Q_A in the up-dip sense. Then, sufficiently far up-dip of the source that the flow has become parallel to the boundary, in the region between the injecting well and the producing well, $x > 0$, mass conservation requires that

$$(H - h)u_1 + hu_2 = Q_I + Q_A, \tag{2.8}$$

while in the region $x < 0$, mass conservation requires that

$$(H - h)u_1 + hu_2 = Q_A. \tag{2.9}$$

Finally, conservation of mass for the ambient fluid gives

$$\phi\frac{\partial h}{\partial t} = -\frac{\partial}{\partial x}(hu_2), \tag{2.10}$$

where ϕ is the porosity of the layer, presumed constant in space and time. By combining these equations and introducing the scalings

$$\tau = \frac{t}{t_s} = \frac{\Delta\rho gk_1\sin\theta}{\mu_1\phi L}t, \quad \xi = \frac{x}{L}, \quad \hat{h} = \frac{h}{H}, \tag{2.11}$$

and the dimensionless parameters

$$M = \frac{k_1\mu_2}{k_2\mu_1}, \quad \Lambda = \frac{Q_I\mu_1}{\Delta\rho g k_1 H \sin\theta}, \quad \Gamma = \frac{Q_A\mu_1}{\Delta\rho g k_1 H \sin\theta}, \quad \epsilon = \frac{H}{L\tan\theta}, \tag{2.12}$$

one finds that the current depth evolves according to the relation

$$\frac{\partial\hat{h}}{\partial\tau} = \frac{\partial}{\partial\xi}\left(\frac{\hat{h}(1-\hat{h})\left(1+\epsilon\dfrac{\partial\hat{h}}{\partial\xi}\right) - (\Lambda+\Gamma)\hat{h}}{M(1-\hat{h})+\hat{h}}\right) \tag{2.13}$$

for the $\xi > 0$ half-space, and the relation

$$\frac{\partial\hat{h}}{\partial\tau} = \frac{\partial}{\partial\xi}\left(\frac{\hat{h}(1-\hat{h})\left(1+\epsilon\dfrac{\partial\hat{h}}{\partial\xi}\right) - \Gamma\hat{h}}{M(1-\hat{h})+\hat{h}}\right) \tag{2.14}$$

for the $\xi < 0$ half-space.

We note that, strictly speaking, the flow is two-dimensional in the near neighbourhood of the wells, $x \sim H$, i.e. $\xi \sim H/L \ll \epsilon$, as the flow adjusts to become parallel to the boundary (cf. Pritchard 2007, § 2.1). However, in the limits (2.1) and (2.3), which correspond to $\Lambda\tan\theta, \Gamma\tan\theta \ll 1$, the change in the depth of the current across this region is negligible, and so we approximate the flow as being described by (2.13) and (2.14) everywhere.

The choice of scalings (2.11) has the advantage that $\phi\Lambda$ and $\phi\Gamma$ are proxies for the injection flux and the aquifer flux, both scaled relative to the buoyancy-driven flow of the injected fluid along the aquifer:

$$\phi\Lambda = Q_I\frac{t_s}{HL}, \quad \phi\Gamma = Q_A\frac{t_s}{HL}. \tag{2.15}$$

This allows an intuitive physical interpretation of the parameters Λ and Γ. In the above, M is the mobility ratio; and ϵ is the ratio of the depth of the layer to the vertical offset between the wells (see figure 1). In this paper, we consider cases where $\epsilon \ll 1$.

Equations (2.13) and (2.14) can be rewritten as a pair of nonlinear advection–diffusion equations:

$$\frac{\partial\hat{h}}{\partial\tau} + f_{\pm}(\hat{h})\frac{\partial\hat{h}}{\partial\xi} - \epsilon\frac{\partial}{\partial\xi}\left(\frac{\hat{h}(1-\hat{h})}{M(1-\hat{h})+\hat{h}}\frac{\partial\hat{h}}{\partial\xi}\right) = 0, \tag{2.16}$$

where

$$f_+(\hat{h}) = -\left(\frac{(M-1)\hat{h}^2 - 2M\hat{h} + M(1-(\Lambda+\Gamma))}{(M(1-\hat{h})+\hat{h})^2}\right) \tag{2.17}$$

describes the advective behaviour for $\xi > 0$, and

$$f_-(\hat{h}) = -\left(\frac{(M-1)\hat{h}^2 - 2M\hat{h} + M(1-\Gamma)}{(M(1-\hat{h})+\hat{h})^2}\right) \tag{2.18}$$

describes the advective behaviour for $\xi < 0$. The third term in (2.16) represents the nonlinear diffusive-type spreading of the current, which originates from the component of gravity normal to the direction of flow.

3. Analytical solutions

In the limit $\epsilon \ll 1$, as considered in this paper, the diffusive term in (2.16) is small and may be neglected except in the event that the nonlinear advective forcing leads to a localized transition in the depth of the flow, in which case the diffusion term may act to smooth this forcing over a length scale $\xi \sim O(\epsilon)$. In dimensional terms, this implies a transition zone that extends along-slope over a distance x that scales as

$$x \sim \frac{H}{\tan\theta} \gg H, \tag{3.1}$$

so the parallel-flow assumption still applies in these transition zones.

We can therefore gain some insight into the expected behaviour of the system at long times by considering solutions of the advection equations

$$\frac{\partial \hat{h}}{\partial \tau} + f_{\pm}(\hat{h})\frac{\partial \hat{h}}{\partial \xi} = 0, \tag{3.2}$$

which have been formed by neglecting the diffusion term in (2.16). We will examine the propagation of surfaces of constant depth as given by the characteristics of these advection equations. Equations (3.2) have characteristic lines given by

$$\hat{h} = \hat{h}_0, \quad \xi = f_{\pm}(\hat{h}_0)\tau. \tag{3.3}$$

In regions in which the characteristics diverge, the current spreads and the gradient $\partial\hat{h}/\partial\xi$ becomes smaller with time. However, in regions in which the characteristics converge, the front of the current tends to steepen, leading to a balance between this steepening and the diffusive spreading associated with the component of gravity normal to the flow.

In order to proceed, we now explore how the speed of the characteristics varies with their depth for different values of Λ and Γ. We identify conditions under which characteristics up-dip of the source migrate up-dip, and similarly under which characteristics down-dip of the source migrate down-dip, in order to identify the long-time structure of the current far from the source. For both the up-dip and the down-dip branches of the current, in the case that the speed of the characteristics decreases with distance from the upper boundary, the depth of the leading edge of the flow decreases smoothly to zero. In the case that the characteristics converge, i.e. the speed of the characteristics increases with distance from the upper boundary, the leading edge of the flow develops a steadily travelling shock-type solution, the structure of which can be described by balancing the diffusive spreading associated with the component of gravity normal to the slope with the along-slope steeping of characteristics. Typically the maximum depth of the branch of the current that propagates up-dip differs from that of the branch of the current that propagates down-dip. We illustrate how the current adjusts from one branch to the other across a quasi-steady region near to the source, which is controlled by a balance between the along-slope advection of characteristics and the diffusive spreading associated with the component of gravity normal to the slope.

It will be seen that the system exhibits seven different regimes of flow, depending on the strength of the aquifer flow and the injection flux, numbered cases (i)–(vii). The

regions of parameter space that give rise to each case, which we will determine in this section, are illustrated in figure 4. Examples of the evolution of currents in each of the cases are shown in § 4.

As we describe below, we find that in some of these cases all the injected fluid flows up-dip, and in some cases all the injected fluid flows down-dip, but in other cases the injected fluid divides, with a fraction moving up-dip and the remainder flowing down-dip. In these cases where the current divides into branches, we assume that the depth of the flow in the vicinity of the source is continuous.

3.1. *Cases (i) and (ii) – strong down-dip aquifer flow*

If the aquifer flux is sufficiently strong in a down-dip sense such that

$$\Lambda + \Gamma < -\frac{1}{M}, \tag{3.4}$$

then the characteristics in the $\xi > 0$ half-space are predicted to propagate down-dip, $f_+(\hat{h}) < 0$ for all $\hat{h}$ (as in the example case $\Lambda + \Gamma = -0.3$ in figure 2). We therefore expect that, at long times, all injected flux will be swept down-dip. Indeed, it can be shown that (3.4) also implies that $f_-(\hat{h}) < 0$ for all $\hat{h}$, meaning that all characteristics in the down-dip half-space tend to propagate down-dip. However, we note that at early time there is a transient up-dip flow associated with the formation of a stationary volume of fluid across which the current depth decreases to zero. Except at the leading edge, the down-dip current has a fixed depth $1 - \hat{h}_{p-}$, which may be calculated by considering the total flux of the current:

$$\Lambda = -\int_{\hat{h}_{p-}}^{1} f_-(\hat{h})\,\mathrm{d}\hat{h}. \tag{3.5}$$

In the case $f'_-(\hat{h}) < 0$, the characteristics are diverging: characteristics for higher values of $\hat{h}$ are swept downstream faster than characteristics for lower values of $\hat{h}$, so the leading edge of the current adjusts smoothly to zero. This occurs if

$$\Gamma < \frac{-1}{M-1}. \tag{3.6}$$

The regime in which (3.4) and (3.6) are satisfied is denoted flow regime (i). In this case the advection equation (3.2) admits a similarity solution as a function of the similarity variable $\eta = \xi/\tau$, given by

$$\hat{h}(\eta) = \frac{M}{M-1}\left(1 - \sqrt{1 - \frac{\eta + \dfrac{1}{M}(1-\Gamma)}{\eta + \dfrac{1}{M-1}}}\right), \tag{3.7}$$

and this describes the structure of the leading edge of the flow in the region $\eta_1 < \eta < \eta_2$ where $\hat{h}(\eta_2) = \hat{h}_{p-}$ and $\eta_1 = 1 + M\Gamma$ is the location of the leading edge of the down-dip branch of the current, $\hat{h} = 1$.

If $\Gamma > -1/(M-1)$, the characteristics converge and the leading edge of the current develops a travelling shock solution: we refer to this as flow regime (ii). The structure of the down-dip leading edge is now described by a steady travelling wave solution of the form $\hat{h} \equiv \hat{h}(\zeta = \xi - C\tau)$ where mass conservation requires that $\Lambda = C(1 - \hat{h}_{p-})$, and $\hat{h}_{p-}$ is calculated using (3.5).

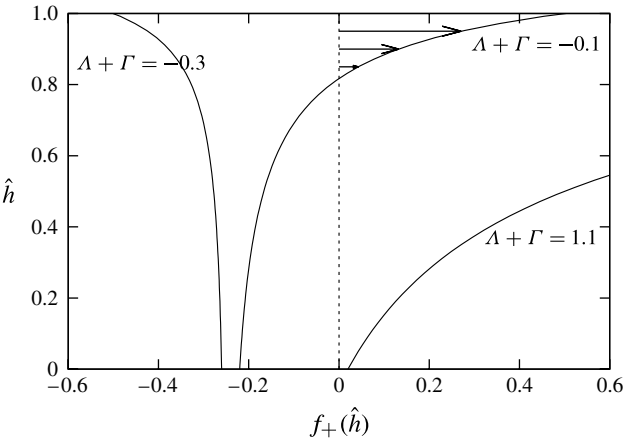

FIGURE 2. Speed of characteristics $f_+(\hat{h})$ (horizontal axis) as a function of $\hat{h}$ (vertical axis) for three values of $\Lambda + \Gamma$, for $M = 5$. In the case $\Lambda + \Gamma = -0.3$, the condition (3.4) is satisfied, so all characteristics tend to propagate down-dip, and so no injectate can propagate up-dip in this case. In the case $\Lambda + \Gamma = -0.1$, some characteristics tend to propagate up-dip and some down-dip. The up-dip propagating characteristics for this case are illustrated by arrows: these are the heights at which injectate can propagate up-dip for this case. (In general, though, injectate will not propagate up-dip at all heights for which the characteristics propagate up-dip, as the injected flux may be insufficient to realize the characteristic curves at all heights.) In the case $\Lambda + \Gamma = 1.1$, the condition (3.18) is satisfied, and the characteristics tend to propagate up-dip for all heights $0 \leqslant \hat{h} \leqslant 1$.

For both of these regimes there is a stationary volume of fluid up-dip from the source across which the depth of the current adjusts to zero (cf. § 4). Here the gravitational force associated with the diffusive spreading of this volume is matched by the down-dip pressure gradient associated with the background flow, as given by the steady-state balance of (2.16) with zero flux. This transition zone extends over a distance $\xi \sim O(\epsilon)$, that is, in dimensional terms, $x \sim H/\tan\theta \gg H$. Therefore the shape of the current may be found by solving the ordinary differential equation

$$\frac{\mathrm{d}\xi}{\mathrm{d}\hat{h}} = -\epsilon \frac{\hat{h}}{M(\Lambda + \Gamma) + \hat{h}}. \tag{3.8}$$

For the boundary condition for this equation, we apply the continuity condition

$$\hat{h}(0) = \hat{h}_{p-}. \tag{3.9}$$

See the start of this section for a discussion of the applicability of the governing equations in the near vicinity of the origin.

3.2. *Cases (iii) and (iv) – stronger influx with down-dip aquifer flow*

We now consider the case where $\Lambda + \Gamma > -1/M$, for which the injected flux is sufficiently large that it can overcome the down-dip aquifer flow, so that there is now a component of injected fluid migrating up-dip of the source, in addition to the down-dip component (figure 3). Analysis of the characteristics for the up-dip current identifies that if $\Gamma + \Lambda < 1$ there is a region $0 < \hat{h} < \hat{h}_*$ for which $f_+(\hat{h}) < 0$, and so the up-dip branch of the current is unable to flood the whole depth of the aquifer (as

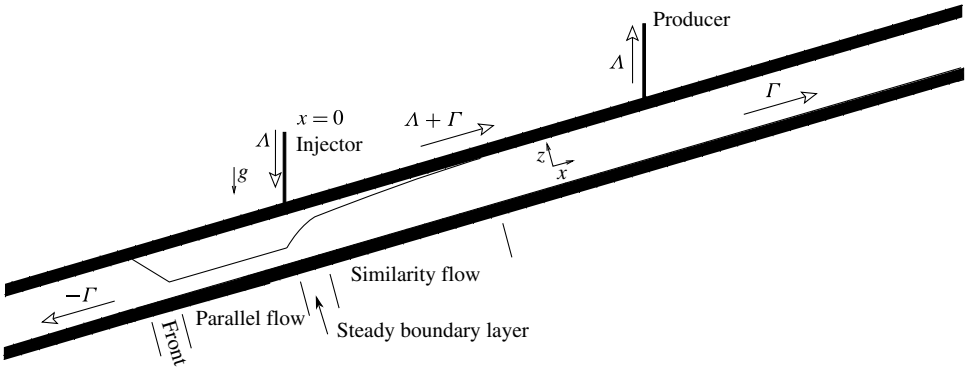

FIGURE 3. Schematic of current in regime (iii) or (iv). These are currents for which $-1/M < \Lambda + \Gamma < 1$ and $\Lambda > \Lambda_C$. Injectate flows into both the up-dip and down-dip half-spaces, but the layer is not flooded with injectate. Note that, as Γ is negative, the down-dip flux in the down-dip sense is positive, with value $-\Gamma$. The down-dip current flows as a current of constant depth, its base parallel to the base of the layer, behind a front (which is a sharp front for currents in regime (iv) and a similarity front (3.7) for currents in regime (iii)). The up-dip current is described by the similarity solution (3.10), and there is a steady boundary layer (3.16) of fixed width immediately up-dip from the injecting well which allows the current to adjust from the depth $\hat{h}_{p-}$ to the depth of the similarity current. Currents in regimes (i) and (ii) are identical to currents in regimes (iii) and (iv) except that they do not have the up-dip similarity current: they have no net up-dip flux after transient behaviour. They still have the steady boundary layer, however, giving a smooth transition from $\hat{h} = \hat{h}_{p-}$ to $\hat{h} = 1$.

in the example case $\Lambda + \Gamma = -0.1$ in figure 2). In the next section we consider the case of even stronger injection $\Lambda + \Gamma > 1$, which leads to full flooding of the aquifer, cases (v) and (vi) of figure 4.

The down-dip branch of the current in regimes (iii) and (iv) is directly analogous to that associated with regimes (i) and (ii), except that the down-dip flux is now only a fraction of the total injected flux. The remainder of the flux now advances up-dip, and in this region the advection equation (2.16) admits a similarity solution for the flow as a function of $\eta = \xi/\tau > 0$ of the form

$$\hat{h} = \frac{M}{M-1}\left(1 - \sqrt{1 - \frac{\eta - \dfrac{1}{M}(\Lambda + \Gamma - 1)}{\eta + \dfrac{1}{M-1}}}\right) \tag{3.10}$$

(cf. the self-similar solutions of Verdon & Woods (2007)). We can understand the origin of this solution by considering the gradient of the speed of the up-dip propagating characteristics:

$$f'_+(\hat{h}) = 2M\left(\frac{(\Lambda + \Gamma)(M-1) + 1}{(M - \hat{h}(M-1))^3}\right). \tag{3.11}$$

For $M > 1$, this is always positive if

$$\Lambda + \Gamma > \frac{-1}{M-1}, \tag{3.12}$$

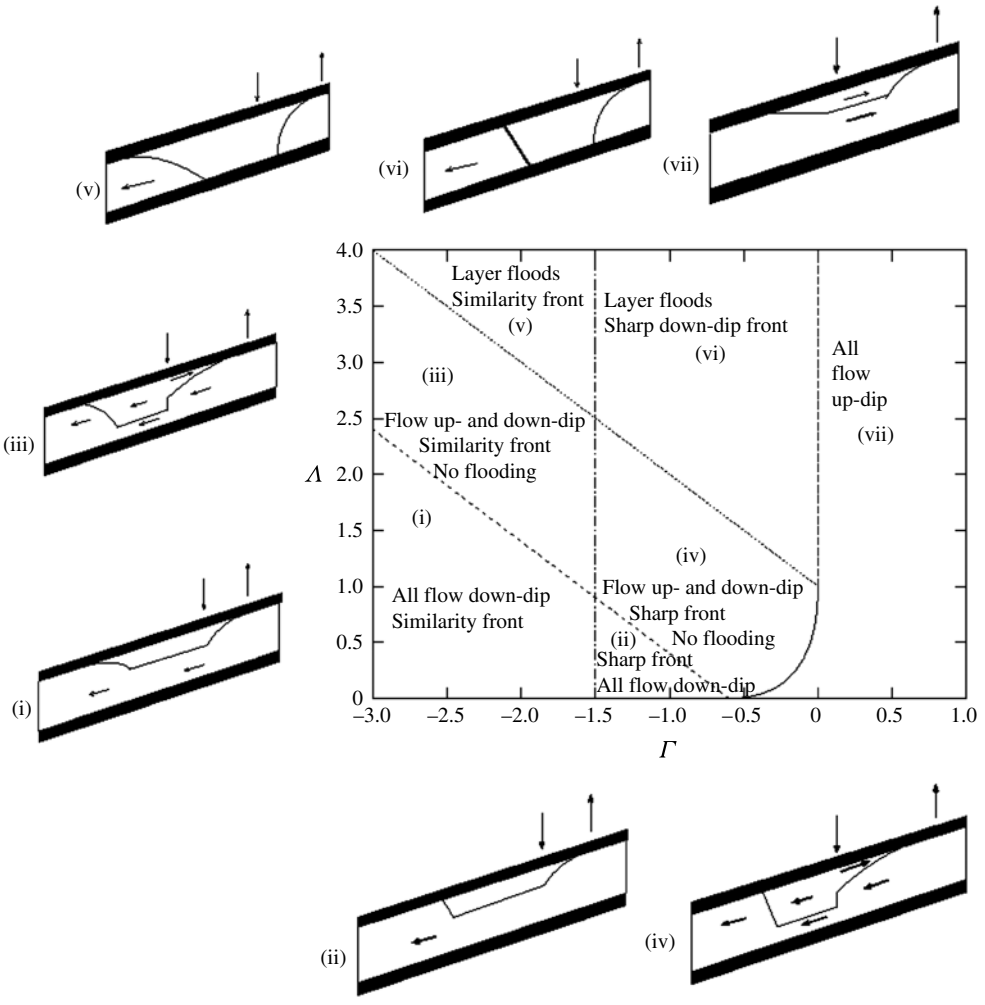

FIGURE 4. Possible flow regimes as a function of Λ and Γ for the case $M = 5/3$. Note that this value of M has been chosen for the purpose of making a clear diagram. For a CO_2–water or CO_2–oil system, M would be much larger, and hence regimes (i), (iii) and (v) would occur for much smaller magnitudes of Γ. The line $\Gamma = 0$ corresponds to the system considered in Gunn & Woods (2011, §3). Regimes in which the layer floods are separated from regimes in which there is flow up- and down-dip without flooding by the line $\Lambda + \Gamma = 1$ (3.18). Regimes in which all flow is down-dip are separated from regimes in which there is flow up- and down-dip by the line $\Lambda + \Gamma = -1/M$ (3.4). Regimes in which there is a similarity front in the down-dip direction are separated from regimes in which there is a sharp front in the down-dip direction by the line $\Gamma = -1/(M-1)$ (3.6). The regime in which all flow is up-dip is separated from the regimes in which there is down-dip flow by the line $\Gamma = 0$ in $\Lambda > 1$ and by $\Lambda < \Lambda_C(\Gamma)$ in $\Lambda < 1$ (3.15).

and (3.12) is always satisfied if $\Lambda + \Gamma > -1/M$ (for $M > 1$; we do not consider cases where $M \leqslant 1$). Therefore, whenever there is a flow of injected fluid into the up-dip half-space, $\Lambda + \Gamma > -1/M$, (3.11) indicates that characteristics associated with higher values of $\hat{h}$ will tend to propagate up-dip faster than characteristics associated

with lower values of $\hat{h}$. We therefore expect a smooth front stretching into $\xi > 0$ with lateral extent in proportion to τ for all cases except (i) and (ii). Equation (3.10) is a precise solution of the advection equation (3.2), and will be a good approximation to the solution of the full advection–diffusion equation if ϵ is small.

The flux in the up-dip branch of the solution has value

$$\Lambda_{up\text{-}dip} = \int_{\hat{h}_{min}}^{1} f_+(\hat{h})\,\mathrm{d}\hat{h}. \tag{3.13}$$

where $\hat{h}_{min}$ is the height of the characteristic that propagates with zero speed. This is calculated from (3.10), as the value for $\hat{h}$ at $\eta = 0$. (Note though that this solution does not describe the flow in the near vicinity of the origin.)

If the injection flux Λ is so small that $\Lambda < \Lambda_{up\text{-}dip}$, then there is no down-dip flow and the flow is in regime (vii) – see § 3.4. Otherwise, the flow is in regime (iii) or (iv) and the remaining flux $\Lambda - \Lambda_{up\text{-}dip}$ then determines the depth of the down-dip current $1 - \hat{h}_{p-}$ according to

$$\Lambda - \Lambda_{up\text{-}dip} = -\int_{\hat{h}_{p-}}^{1} f_-(\hat{h})\,\mathrm{d}\hat{h}, \tag{3.14}$$

analogous to regimes (i) and (ii). The minimum value Λ_C for which some flux migrates down-dip evaluates to

$$\Lambda_C = \left(1 - \sqrt{-M\Gamma}\right)^2. \tag{3.15}$$

Case (iii), in which there is a smooth down-dip front, is separated from case (iv), in which there is a sharp down-dip travelling front, by the condition (3.6), just as for cases (i) and (ii).

In these solutions we find that the depth of the down-dip current $1 - \hat{h}_{p-}$ exceeds the maximum depth of the up-dip current. Therefore, in the region just up-dip of the source, the current depth decreases from $1 - \hat{h}_{p-}$ to $1 - \hat{h}(0)$, which is the depth above which all characteristics in $\xi > 0$ propagate up-dip (see (3.10)). The adjustment is governed by the steady balance between the down-dip advection of characteristics for $\hat{h} < \hat{h}(0)$ in $\xi > 0$, and the up-dip gravitational spreading of the flow associated with the component of gravity normal to the slope, as given by (2.16). In the adjustment region there is a net upward flux $\Lambda_{up\text{-}dip}$. Using this to give the constant of integration, and integrating the governing equation, gives an equation for the variation of depth in the transition region,

$$\frac{\mathrm{d}\xi}{\mathrm{d}\hat{h}} = \epsilon \frac{\hat{h}(1-\hat{h})}{\Lambda_{up\text{-}dip}(M - h(M-1)) + (\Lambda + \Gamma)\hat{h} - \hat{h}(1-\hat{h})}, \tag{3.16}$$

where the boundary condition for this equation is

$$\hat{h}(0) = \hat{h}_{p-}, \tag{3.17}$$

as before (cf. figure 8*a*).

3.3. *Cases (v) and (vi)*

If the injection flux is sufficiently strong relative to the aquifer flux that

$$\Lambda + \Gamma > 1, \tag{3.18}$$

then $f_+(\hat{h})$ is always positive, meaning that characteristics for all values of $\hat{h}$ tend to propagate up-dip (as in the example case $\Lambda + \Gamma = 1.1$ illustrated in figure 2). If $\Gamma > 0$ then ambient fluid also propagates up-dip, so the injectate does not fill the entire depth of the aquifer. However, if $\Gamma < 0$ and (3.18) is satisfied, then the aquifer flux is of smaller magnitude than the injection flux, but with a down-dip sense. As a result, all the aquifer flow originating from up-dip is extracted by the producing well, while near the injection well the injectate floods the whole depth of the aquifer and divides into a component that flows up-dip towards the producing well and a component that migrates down-dip with flux $-\phi\Gamma$ in $\xi < 0$, corresponding to the background aquifer flow that is extracted from the up-dip producing well, as required by mass conservation. This corresponds to regimes (v) and (vi) of figure 4. The solution up-dip is given by the similarity solution (3.10), which extends from $\hat{h} = 0$ to $\hat{h} = 1$, and the solution down-dip is either the smooth front as given by (3.7) (regime (v)) or a shock front (regime (vi)), depending on whether (3.6) is satisfied.

3.4. *Case (vii)*

In this regime all injected flux propagates up-dip. This occurs when there is a very weak down-dip aquifer flow and a very weak injection flow, or when there is an up-dip aquifer flow. The flow is in this regime if $\Gamma > 0$ or $\Lambda < \Lambda_C$, where Λ_C is given by (3.15). Mass conservation determines the depth of the current according to the relation

$$\Lambda = \int_{\hat{h}_{p+}}^{1} f_+(\hat{h})\,\mathrm{d}\hat{h}. \tag{3.19}$$

which gives

$$\Lambda = \frac{(M\Gamma + \hat{h}_{p+})(1 - \hat{h}_{p+})}{\hat{h}_{p+}}. \tag{3.20}$$

The flow thus has a region of constant depth $1 - \hat{h}_{p+}$, with a smooth leading edge described by the similarity solution (3.10), which applies in the region $\eta_1 < \eta < \eta_2$ where (3.10) gives $\hat{h}(\eta_1) = \hat{h}_{p+}$ and $\hat{h}(\eta_2) = 1$.

In case (vii) there is now a standing body of fluid down-dip from the source, as given by the steady-state solution of (2.16) for the down-dip half-space, with no flux.

3.5. *Special case*

The possible behaviours of the system as a function of Λ and Γ for the example case $M = 5/3$ are summarized in figure 4. The line $\Gamma = 0$ corresponds to the system considered in Gunn & Woods (2011, § 3). When $\Gamma = 0$ and $\Lambda < 1$, all flow of injectate is up-dip. The case $\Gamma = 0$ and $\Lambda > 1$ is special, corresponding to the boundary between two regimes. Gunn & Woods (2011) found that in this case the layer does flood to its base with injectate, but that no injectate propagates down-dip after initial transient behaviour: asymptotically, all flow of injectate is up-dip. It is informative to note that any background flow, though it may be arbitrarily small, will move the system out of this special case and either into a regime in which injectate propagates down-dip, or one in which ambient fluid propagates up-dip past $\xi = 0$.

4. Numerical illustration and discussion of physics

In this section we will illustrate the transient adjustment to the asymptotic solutions of § 3. The numerical integration of the governing equations (2.13) and (2.14) also

serves as a check of the analytical predictions for the long-time behaviour. We will briefly discuss the numerical technique involved; then we will show some results from the numerical integration, which will serve to illustrate both the agreement with the analytical results, and the nature of the different regimes. We will discuss the physical meaning of the values of Λ and Γ to give insight into the physical origins of the different regimes.

4.1. *Numerical method*

The equations were integrated using a Crank–Nicolson scheme (Press *et al.* 1992), with the boundary condition at the injection well $\xi = 0$ being that the depth of the current is continuous, as was assumed for the analytical solutions.

In our numerical calculations, the inflow is initially partitioned equally between the up-dip ($\xi > 0$) and down-dip ($\xi < 0$) half-spaces, as suggested by the limit of (2.13) and (2.14) at $\tau = 0$ and near the injection point $\xi = 0$. Subsequently, the partitioning of the injected flux between the up-dip and down-dip domains evolves in order to ensure that continuity of $\hat{h}$ at the origin is satisfied. Note that in regimes (i) and (ii), once the layer has flooded to its base, continuity is automatically satisfied, as $\hat{h}(0^+) = \hat{h}(0^-) = 0$. In these cases, the partitioning chosen is $Q_{down\text{-}dip} = -Q_A$, in order to satisfy the requirement of incompressibility. In all other cases, the partitioning is calculated as follows. At each time step, a partitioning of Q_I into $Q_{up\text{-}dip}$ and $Q_{down\text{-}dip}$ is postulated. A value for $\hat{h}(0)$ is then calculated from the partitioning as follows. For the up-dip half-space, we combine

$$Q_{up\text{-}dip} = (H - h(0))u_1(0) \tag{4.1}$$

and

$$Q_I + Q_A - Q_{up\text{-}dip} = h(0)u_2(0) \tag{4.2}$$

with (2.6) and (2.7) to give a boundary value for $\partial\hat{h}/\partial\xi(0)$ as a function of the postulated values of $\hat{h}(0)$ and $Q_{up\text{-}dip}$. An equivalent condition is made for the down-dip half-space. An iterative relaxation method is used in each half-space to find a pair of values for $\hat{h}(0)$ and $\partial\hat{h}/\partial\xi(0)$ for the next time step that satisfy (2.6), (2.7), (4.1) and (4.2), or the equivalent for the down-dip half-space. If the values of $\hat{h}(0)$ obtained by this process for each half-space agree within a small error, this solution is taken as the solution for the next time step; if not, then a new partitioning is postulated by interval bisection and the process is repeated.

In this calculation, it is possible that points near the nose or base of the front overshoot $\hat{h} = 1$ or $\hat{h} = 0$, taking values $\hat{h} > 1$ or $\hat{h} < 0$. Therefore, after the solution for each new time step is calculated, we set the value of $\hat{h}$ to equal 1 or 0, respectively, wherever it has taken a value greater than 1 or less than 0. This is the only special treatment given to the points $\hat{h} = 0$ and $\hat{h} = 1$. We find in the numerics that the gradient of $\hat{h}$ does not tend to become infinite at these points, as is consistent with our analytical solutions (§ 3). We have tested our numerical results for robustness, finding that halving the space and time steps gives the same result, and in particular we have sufficient resolution to fully resolve the adjustment of the flow to zero depth at the nose.

Note that it is only through the boundary condition at the origin that the partitioning of the injected flux has an effect on the solution, as the governing equations (2.13) and (2.14) have no dependence on the partitioning of the flux.

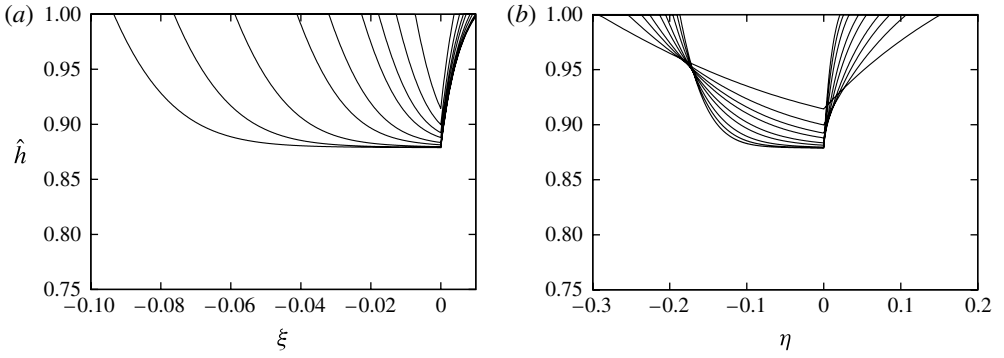

FIGURE 5. Evolution of the flow for the case $\Lambda = 0.02$, $\Gamma = -0.225$ and $M = 5$. Here $\hat{h}$ is plotted (*a*) as a function of ξ and (*b*) as a function of the similarity variable η, for the times $\tau = 0.025, 0.05, 0.075, 0.1, 0.15, 0.2, 0.3, 0.4$ and 0.5. Panel (*a*) illustrates that, up-dip from the point of injection, the injected fluid rapidly forms a stationary interface with the original fluid. Note the vertical axis has the range $0.75 \leqslant \hat{h} \leqslant 1$, because the current is confined to the top of the aquifer.

4.2. *Illustrations and discussion*

We now provide illustrative figures showing the numerical prediction of the evolution of one example current for each of the seven regimes illustrated in figure 4.

4.2.1. *All flow down-dip; regimes (i) and (ii)*

In this case the aquifer flux is sufficiently strong (in the down-dip sense) that all injected flux is swept down-dip. In regime (ii) the aquifer flux is still sufficiently weak that the front of the current of injectate is buoyancy-stabilized, and in this regime there is no over-riding finger of less viscous fluid running down-dip along the top of the layer. An example of a current in regime (ii) is shown in figure 5. In regime (i) the background flux is sufficiently strong that the front of the current of injectate is no longer buoyancy-stabilized, and a thin finger of the less-viscous injectate develops along the top of the layer in the down-dip direction. A current in regime (i) is shown in figure 6.

4.2.2. *Flow up-dip and down-dip without flooding; regimes (iii) and (iv)*

In regime (iv), as in regime (ii), the background flux is sufficiently weak that the front of the down-dip current of injectate is buoyancy-stabilized. Regime (iii) corresponds to regime (i) in having a similarity front in the down-dip direction. In regimes (iii) and (iv), however, the larger value of injected flux Λ means that there is now also a flux of injectate up-dip, against the background flow. Figure 7 shows the evolution of an example current with the same values of Γ and M as in figure 5 but with a higher value of Λ. Figure 8 shows the evolution of a current with the same values of Γ and M as in figure 6, but with a higher value of Λ. Figure 8(*a*) illustrates the steady adjustment of the current from the down-dip region $\xi < 0$ to the shallower up-dip self-similar flow, as determined by the advection–diffusion balance (3.16). Note that the horizontal axis of figure 8(*a*) shows ξ, the scaled x coordinate, whereas the horizontal axis of figure 8(*b*) shows the similarity coordinate η.

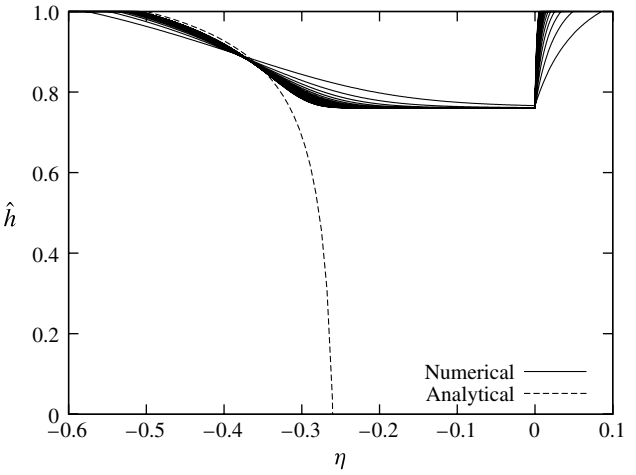

FIGURE 6. Evolution of the flow for the case $\Lambda = 0.1$, $\Gamma = -0.3$ and $M = 5$. Plot of $\hat{h}$ as a function of the similarity variable η. The figure illustrates the convergence to the similarity solution (3.7) in $x < 0$. The analytical similarity solution exists for all heights. However, in regimes for which there is insufficient injected flux to flood the layer to its base, the current of injectate forms a current along the top of the layer, and the front of the current conforms to the similarity solution only within the depth of the current, $\hat{h}_{p-} < \hat{h} < 1$. Characteristics associated with lower heights still tend to propagate down-dip, but there is insufficient injectate for this to be physically realized.

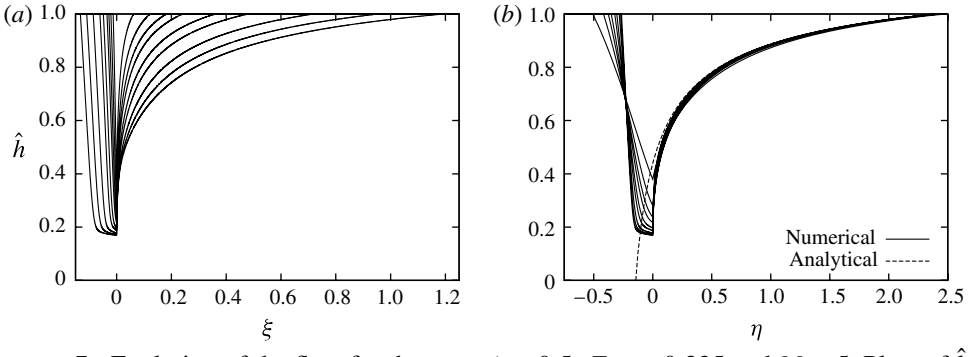

FIGURE 7. Evolution of the flow for the case $\Lambda = 0.5$, $\Gamma = -0.225$ and $M = 5$. Plots of $\hat{h}$ as a function of (*a*) ξ and (*b*) η, for times $\tau = 0.025, 0.05, 0.075, 0.1, 0.15, 0.2, 0.3, 0.4$ and 0.5. Panel (*b*) illustrates the convergence to the similarity solution (3.10) in $x > 0$.

4.2.3. *Layer floods; regimes (v) and (vi)*

For yet higher values of injected flux Λ, the layer floods to its base, and injectate flows into both the up-dip and the down-dip half-spaces at all heights. However, for sufficiently weak background flux, the front of the down-dip current is still buoyancy-stabilized: this is regime (vi), and an example of this regime is illustrated in figure 9. Figure 9 uses again the same values of Γ and M used in figures 7 and 5, but with a yet higher value of Λ. Regime (v) occurs when both injected flux and down-dip aquifer flux are strong (large values of Λ, negative values of Γ of large magnitude). Figure 10 shows the evolution of an example current in this regime, showing the

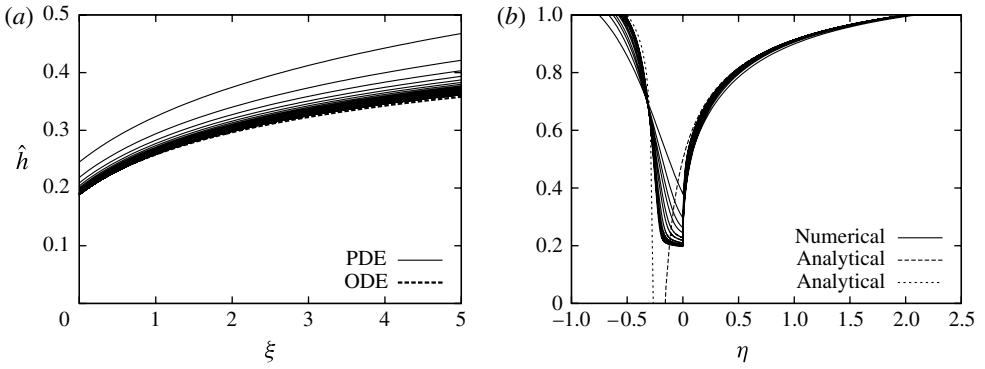

FIGURE 8. Evolution of the flow for the case $\Lambda = 0.5$, $\Gamma = -0.3$ and $M = 5$. (*a*) Evolution of the flow as a function of ξ for times $\tau = 0.1, 0.2, \ldots, 5$, with the inner solution (3.16) shown for comparison. (*b*) Plot of $\hat{h}$ as a function of the similarity variable η for times $\tau = 0.025, 0.05, 0.075, 0.1, 0.15, 0.2, 0.3, 0.4, 0.5, 0.6$ and 0.7. The figure illustrates the convergence to the similarity solution (3.10) in $x > 0$, and to (3.7) in $x < 0$.

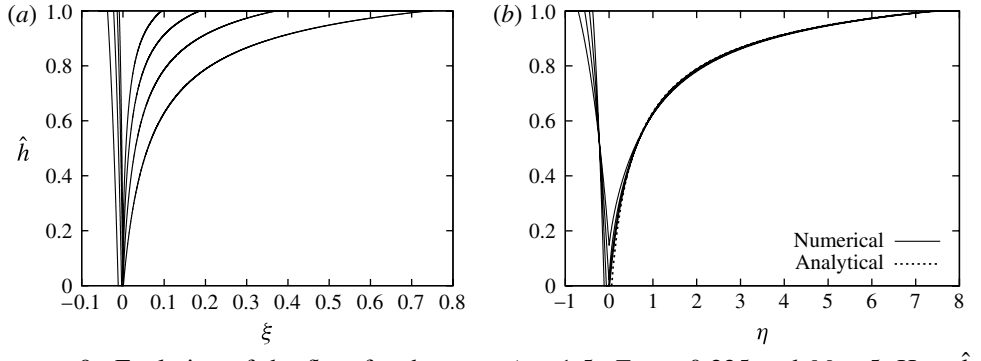

FIGURE 9. Evolution of the flow for the case $\Lambda = 1.5$, $\Gamma = -0.225$ and $M = 5$. Here $\hat{h}$ is plotted as a function of (*a*) ξ and (*b*) η, for times $\tau = 0.0125, 0.025, 0.05$ and 0.1. Panel (*b*) illustrates the convergence to the similarity solution (3.10) in $x > 0$.

flooding of the layer close to the injection point $\xi = 0$ and the similarity fronts in both the up-dip and down-dip directions.

4.2.4. *All flow up-dip; regime (vii)*

If $\Gamma > 0$, then all flow of injected flux is up-dip, as in this case both buoyancy and pressure forces tend to act to cause the injectate to flow up-dip (an example is shown in figure 11). It is also possible for all injectate to flow up-dip for small negative values of Γ, provided the injected flux is sufficiently small, so that the buoyancy effect dominates.

5. Down-dip producing well

We now examine the different situation in which the producing well is located down-dip from the injecting well. This leads to a modified set of governing equations. The mass-conservation equations (2.8) and (2.9) are now replaced by the relations

$$(H - h)u_1 + hu_2 = Q_A \tag{5.1}$$

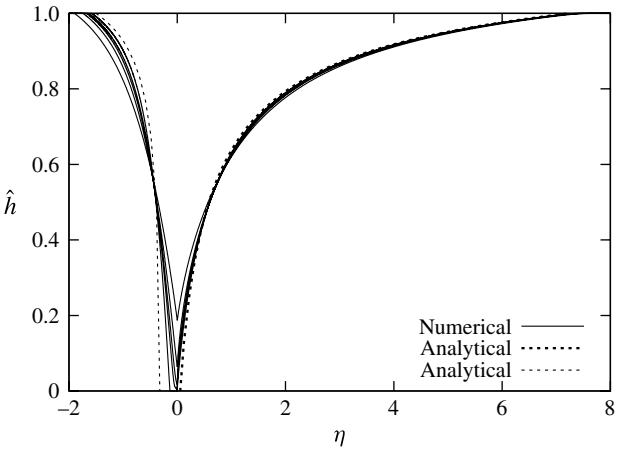

FIGURE 10. Evolution of the flow for the case $\Lambda = 1.75$, $\Gamma = -0.5$ and $M = 5$. Plot of $\hat{h}$ as a function of the similarity variable η for times $\tau = 0.0625, 0.0125, 0.025$ and 0.05. The figure illustrates the convergence to the similarity solution (3.10) in $x > 0$ and to (3.7) in $x < 0$.

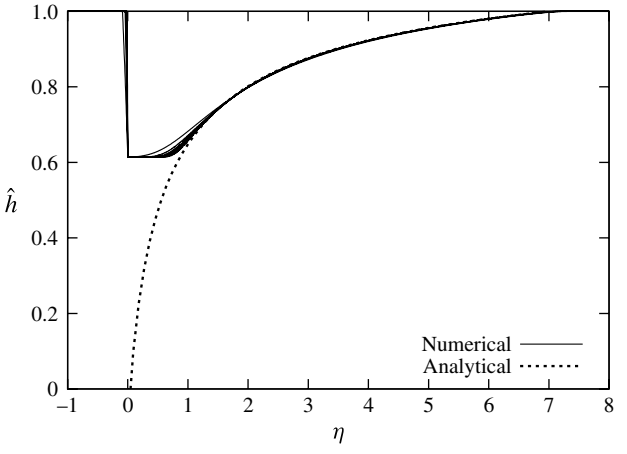

FIGURE 11. Evolution of the flow for the case $\Lambda = 1$, $\Gamma = 0.2$ and $M = 5$. Plot of $\hat{h}$ as a function of the similarity variable η for times $\tau = 0.0125, 0.025, 0.0375, 0.05$ and 0.1. The figure illustrates the convergence to the similarity solution (3.10) in $x > 0$.

for the region $x > 0$ and

$$(H - h)u_1 + hu_2 = Q_A - Q_I \tag{5.2}$$

for the region $x < 0$. This results in the governing equations

$$\frac{\partial \hat{h}}{\partial \tau} = \frac{\partial}{\partial \xi}\left(\frac{\hat{h}(1-\hat{h})\left(1+\epsilon\dfrac{\partial \hat{h}}{\partial \xi}\right) - \Gamma \hat{h}}{M - \hat{h}(M-1)}\right) \tag{5.3}$$

for the region $\xi > 0$ and

$$\frac{\partial \hat{h}}{\partial \tau} = \frac{\partial}{\partial \xi}\left(\frac{\hat{h}(1-\hat{h})\left(1+\epsilon\dfrac{\partial \hat{h}}{\partial \xi}\right) - (\Gamma - \Lambda)\hat{h}}{M - \hat{h}(M-1)}\right) \tag{5.4}$$

for $\xi < 0$. These equations are identical to the earlier set of governing equations (2.13) and (2.14) under the transformation

$$\Gamma \to \Gamma - \Lambda. \tag{5.5}$$

This may be understood as follows. When in § 2 the production well was up-dip from the injection well, the flux immediately up-dip from the injection well was $\phi\Lambda + \phi\Gamma$, the sum of the flux due to injection and the aquifer background flux. But here the production well is down-dip from the injection well, so the flux up-dip from the injection well is $\phi\Gamma$, the aquifer flux. Similarly, when the production well was up-dip, the down-dip flux was the aquifer flux $\phi\Gamma$. But with the production well down-dip, the flux immediately down-dip from the injection well is $\phi\Gamma - \phi\Lambda$: the injection flux is subtracted because it is has a down-dip sense. So, it can be seen that, when moving from a scenario with the production well up-dip to one with the production well down-dip, the correct change in the flux both up-dip and down-dip from the injection well is produced by the transformation (5.5).

By analogy with § 3, in the small-ϵ limit in which the dynamics are controlled by the along-slope advection, consideration of the propagation speed of the characteristics identifies that there are seven possible flow regimes. Since the analysis is directly equivalent to the approach presented in § 3, we do not repeat all the derivation. However, in figure 12, we illustrate the regime diagram for this system, in the example case $M = 5/3$ (cf. figure 4).

In the case of a down-dip producing well, an up-dip background flow ($\Gamma > 0$) tends to oppose the flow driven by the pressure difference between the injecting and producing wells (proportional to Λ). Thus, when $\Gamma > \Lambda > 0$, the background flux is sufficient to overcome the pressure gradient associated with the wells, and all injected flux flows up-dip. Owing to the buoyancy of the injected fluid, it is also possible for all injected fluid to flow up-dip for some slightly less positive or weakly negative background fluxes. Flooding of the layer to its base occurs where a strong up-dip background flow $\Gamma > 1$ is opposed by a yet stronger injection flux $\Lambda > \Gamma > 1$. In the case of a small down-dip background flow, even though the flow associated with injection/production is aligned with the background flow, some injectate will still tend to flow up-dip due to buoyancy; for all injectate to flow down-dip, a relatively strong down-dip background flow $\Gamma < -1/M$ is required.

6. Discussion and application

We have analysed the motion of a maintained release of buoyant fluid as it spreads through a confined aquifer with a background flow. The modelling has identified some of the key controls on the motion of the current, including the roles of the buoyancy, of the mobility ratio and of the rate of injection. Depending on the dimensionless controlling parameters Γ, Λ and M, the system will exhibit one of seven possible flow regimes.

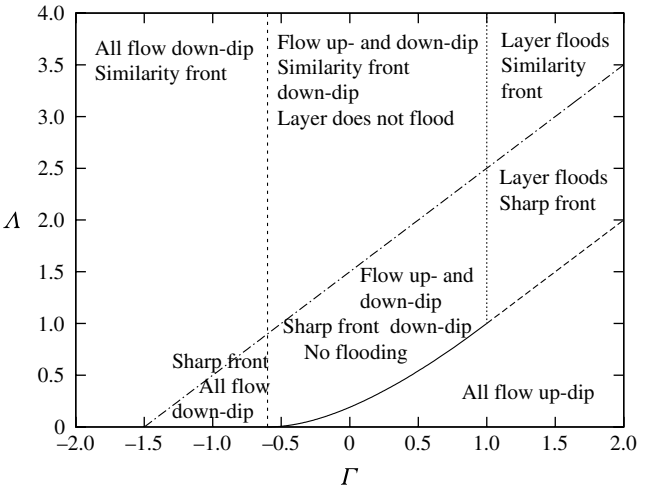

FIGURE 12. Possible flow regimes as a function of Λ and Γ for the case $M = 5/3$. (Note that, as with figure 4, this value of M is smaller than in physical systems.) The line $\Gamma = 0$ corresponds to the system considered in Gunn & Woods (2011, §4). The lines separating the regimes are given by the equations describing the lines separating the equivalent regimes in figure 4 under the transformation (5.5). For example, regimes in which the layer floods are separated from regimes in which the layer does not flood by the line $\Gamma = 1$, cf. the line $\Gamma + \Lambda = 1$ in § 3.

Let us now consider what values of these parameters might be found in a practical CO_2 injection scenario. If a typical aquifer background flow velocity is 10^{-8}–10^{-7} m s^{-1} (Garven 1995), then for an aquifer 10–100 m thick this would correspond to a flux $Q_A = 10^{-7}$–10^{-5} m^2 s^{-1}. For the case of CO_2 displacing water, the relevant physical quantities are $\Delta\rho = 250$ kg m^{-3}, $\mu_1 = 2 \times 10^{-5}$ Pa s and $\mu_2 = 9 \times 10^{-4}$ Pa s. The value of k may be between 10^{-12} m^2, as in the Sleipner field (Bickle *et al.* 2007), and 10^{-14} m^2, as in the case of the In Salah reservoir (Cavanagh & Ringrose 2010). Then, taking $\sin\theta \sim 0.1$, we find that the typical magnitudes of Γ will be in the range $\Gamma = 10^{-5}$–1. If a typical injection flux is $Q_I = 10^{-5}$–10^{-4} m^2 s^{-1} (IPCC 2005), then similarly we expect a range of values of $\Lambda = 10^{-3}$–10.

Our model describes regimes for which $\Lambda, \Gamma \ll 1/\tan\theta$. These values correspond to systems with rock of high permeability, deeper aquifers or lower injection rates. By considering the results illustrated in figure 4, we see that, for the case of a producing well up-dip from the injecting well, any of the regimes we identified may be encountered in physical situations. For small aquifer fluxes, all injected fluid may flow up-dip; there may be flow both up- and down-dip from the point of injection, with a sharp front to the down-dip current, while the layer does not flood to its base; or the layer may flood to its base, with, again, flow both up- and down-dip, and a sharp front to the down-dip current. For larger but still physically plausible values of the aquifer flux, we expect to see regimes for which all flow of injectate is down-dip or for which there is a similarity front to the down-dip flow.

Similarly, all regimes are within the range of physically reasonable systems for the case where the producing well is down-dip from the injecting well (cf. figure 12). We will now consider, in dimensional terms, for which systems we expect to see a similarity front form in the down-dip direction, when the wells are in this configuration. The similarity front forms if $\Lambda > \Gamma + 1/(M-1)$, which, in dimensional

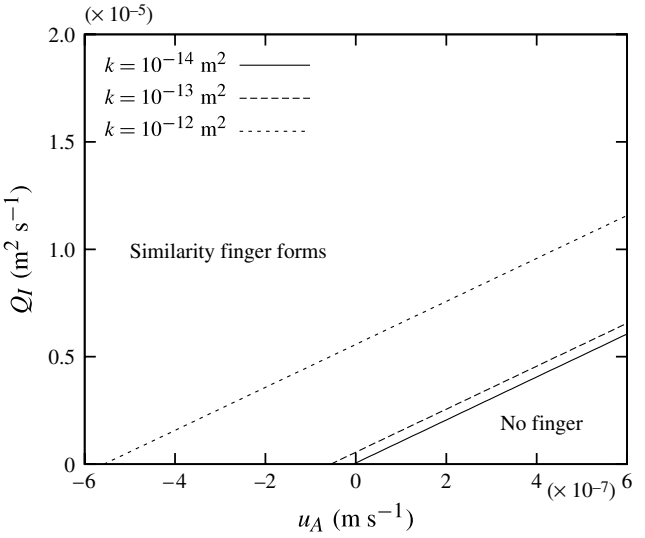

FIGURE 13. Maximum values of Q_I for which no similarity front forms, as a function of background flow velocity. Parameter values used are: $\Delta\rho = 250$ kg m^{-3}, $g = 9.81$ m s^{-2}, $H = 10$ m, $\sin\theta = 0.2$, $\mu_1 = 2 \times 10^{-5}$ Pa s and $\mu_2 = 9 \times 10^{-4}$ Pa s.

terms, is

$$Q_I > Q_A + \frac{\Delta\rho g k H \sin\theta}{\mu_2 - \mu_1} = H u_A + \frac{\Delta\rho g k H \sin\theta}{\mu_2 - \mu_1}. \tag{6.1}$$

Figure 13 shows, for three illustrative values of permeability k, the maximum injection rate at which CO_2 can be injected into a layer without causing early breakthrough of injectate to the down-dip producing well due to the formation of a similarity finger, as a function of aquifer background flow velocity u_A.

Our model is simplified in order to identify the key impacts of the background flow. Several simplifications could be relaxed in subsequent studies. For example, the model could be extended to account for compressibility of the fluids, as the effects of compressibility may become progressively more important for systems in which the distance between the injection well and the far-field fault are increasingly very large. Other extensions could be to consider some of the three-dimensional dynamics and also some of the two-phase flow effects associated with the immiscibility of water and CO_2 (Pruess *et al.* 2003; Hesse *et al.* 2008), heterogeneity of the rock and dissolution of CO_2 in the formation water and other possible reactive effects (cf. Bear 1988; Pruess *et al.* 2003; Nordbotten & Celia 2006).

Acknowledgement

Our research was supported by NERC and by BP plc through the BP Institute.

REFERENCES

BARENBLATT, G. I. 1996 *Dimensional Analysis, Self-Similarity and Intermediate Asymptotics*. Cambridge University Press.

BEAR, J. 1988 *Dynamics of Fluids in Porous Media*. Dover.

BICKLE, M., CHADWICK, A., HUPPERT, H. E., HALLWORTH, M. & LYLE, S. 2007 Modelling carbon dioxide accumulation at Sleipner: implications for underground carbon storage. *Earth Planet. Sci. Lett.* **255**, 164–176.

CAVANAGH, A. & RINGROSE, P. 2010 Salah high-resolution heterogeneous simulations of CO_2 storage. *Search and Discovery*, 80092.

FARCAS, A. & WOODS, A. W. 2009 The effect of drainage on the capillary retention of CO_2 in a layered permeable rock. *J. Fluid Mech.* **618**, 349–359.

GARVEN, G. 1995 Continental-scale groundwater flow and geologic processes. *Annu. Rev. Earth Planet. Sci.* **23**, 89–117.

GUNN, I. & WOODS, A. W. 2011 On the flow of buoyant fluid injected into a confined, inclined aquifer. *J. Fluid Mech.* **672**, 109–129.

HESSE, M. A., ORR, F. M. JR & TCHELEPI, H. A. 2008 Gravity currents with residual trapping. *J. Fluid Mech.* **611**, 35–60.

IPCC 2005 *IPCC Special Report on Carbon Dioxide Capture and Storage*. Cambridge University Press.

JUANES, R., MACMINN, C. W. & SZULCZEWSKI, M. L. 2010 The footprint of the CO_2 plume during carbon dioxide storage in saline aquifers: storage efficiency for capillary trapping at the basin scale. *Transp. Porous Med.* **82**, 19–30.

JUANES, R. E., SPITERI, J., ORR, F. M. & BLUNT, M. J. 2006 Impact of relative permeability hysteresis on geological CO_2 storage. *Water Resour. Res.* **42**, W12418.

MITCHELL, V. & WOODS, A. W. 2006 Gravity driven flow in confined aquifers. *J. Fluid Mech.* **566**, 345–355.

NEUFELD, J. A., HESSE, M. A., RIAZ, A., HALLWORTH, M. A., TCHELEPI, H. A. & HUPPERT, H. E. 2010 Convective dissolution of carbon dioxide in saline aquifers. *Geophys. Res. Lett.* **37**, L22404.

NEUFELD, J. A., VELLA, D. & HUPPERT, H. E. 2009 The effect of a fissure on storage in a porous medium. *J. Fluid Mech.* **639**, 239–259.

NORDBOTTEN, J. M. & CELIA, M. A. 2006 Similarity solutions for fluid injection into confined aquifers. *J. Fluid Mech.* **561**, 307–327.

NORDBOTTEN, J. M., KAVETSKI, D., CELIA, M. A. & BACHU, S. 2009 Model for CO_2 leakage including multiple geological layers and multiple leaky wells. *Environ. Sci. Technol.* **43**, 739–749.

PRESS, W. H., TEUKOLSKY, S. A., VETTERLING, W. T. & FLANNERY, B. P. 1992 *Numerical Recipes in Fortran 77*. Cambridge University Press.

PRITCHARD, D. 2007 Gravity currents over fractured substrates in a porous medium. *J. Fluid Mech.* **584**, 415–431.

PRUESS, K., XU, T., APPS, J. & GARCIA, J. 2003 Numerical modelling of aquifer disposal of CO_2. *SPE J.* **8** (1), 49–60.

VELLA, D. & HUPPERT, H. E. 2006 Gravity currents in a porous medium at an inclined plane. *J. Fluid Mech.* **555**, 353–362.

VERDON, J. & WOODS, A. W. 2007 Gravity driven reacting flows in a confined porous aquifer. *J. Fluid Mech.* **588**, 29–41.

WOODS, A. W. & NORRIS, S. 2010 On the role of caprock and fracture zones in dispersing gas plumes in the subsurface. *Water Resour. Res.* **46**, W08522.

YORTSOS, Y. C. 1995 A theoretical analysis of vertical flow equilibrium. *Trans. Porous Med.* **18**, 107–129.